the corresponding direction cosines η_A and δ_A in the reference system $(OXYZ)_A$. The projections on the absorption plane of the two beams and of their mean direction are characterized by the angles

$$\tan \varepsilon_{\text{inc.}}(\mathbf{h}) = \frac{\eta_{3A}(\mathbf{h})}{\eta_{2A}(\mathbf{h})}, \qquad (A18)$$

$$\tan \varepsilon_{\text{diffr.}}(\mathbf{h}) = \frac{\delta_{3A}(\mathbf{h})}{\delta_{2A}(\mathbf{h})} \qquad (A19)$$

and

$$\tan \varepsilon_{\text{mean}}(\mathbf{h}) = \frac{\eta_{3A}(\mathbf{h}) + \delta_{3A}(\mathbf{h})}{\eta_{2A}(\mathbf{h}) + \delta_{2A}(\mathbf{h})}. \qquad (A20)$$

From these angles we may easily calculate the values of the azimuth at which the absorption reflection **k** has to be measured to carry out the absorption correction with one of the methods analyzed and, from these, the settings of the diffractometer required for the measurement.

References

ARNDT, U. W. & PHILLIPS, D. C. (1961). *Acta Cryst.* **14**, 807–818.

BANNER, D. W., EVANS, P. R., MARSH, D. J. & PHILLIPS, D. C. (1977). *J. Appl. Cryst.* **10**, 45–51.

BUERGER, M. J. (1942). *X-ray Crystallography*, pp. 301–304. New York: John Wiley.

BUSING, W. R. & LEVY, H. A. (1957). *Acta Cryst.* **10**, 180–182.

BUSING, W. R. & LEVY, H. A. (1967). *Acta Cryst.* **22**, 457–464.

CAIN, J. E., NORVELL, J. C. & SCHOENBORN, B. P. (1975). *Neutron Scattering for the Analysis of Biological Structures*, edited by B. P. SCHOENBORN, pp. VIII, 43–50. Report BNL50453. Brookhaven National Laboratory, Upton, NY.

COPPENS, P., LEISEROWITZ, L. & RABINOVICH, D. (1965). *Acta Cryst.* **18**, 1035–1038.

FLACK, H. D. (1974). *Acta Cryst.* A**30**, 569–573.

FURNAS, T. C. (1957). *Single-Crystal Orienter Instruction Manual.* Milwaukee: General Electric Company.

International Tables for X-ray Crystallography (1959). Vol. II, p. 300. Birmingham: Kynoch Press.

KATAYAMA, C., SAKABE, N. & SAKABE, K. (1972). *Acta Cryst.* A**28**, 293–295.

KOPFMAN, G. & HUBER, R. (1968). *Acta Cryst.* A**24**, 348–351.

LEE, B. & RUBLE, J. R. (1977). *Acta Cryst.* A**33**, 629–637.

MEULENAER, J. DE & TOMPA, H. (1965). *Acta Cryst.* **19**, 1014–1018.

NORTH, A. C. T., PHILLIPS, D. C. & MATHEWS, F. S. (1968). *Acta Cryst.* A**24**, 351–359.

PHILLIPS, D. C. (1964). *J. Sci. Instrum.* **41**, 123–129.

PRINCE, E., WLODAWER, A. & SANTORO, A. (1978). *J. Appl. Cryst.* **11**, 173–178.

SANTORO, A. (1969). *Crystallographic Computing*, edited by F. R. AHMED, pp. 283–290. Copenhagen: Munksgaard.

SANTORO, A. & ZOCCHI, M. (1964). *Acta Cryst.* **17**, 597–602.

WELLS, M. (1960). *Acta Cryst.* **13**, 722–726.

XUONG, N. H., FREER, S. T., HAMLIN, R., NIELSEN, C. & VERNON, W. (1978). *Acta Cryst.* A**34**, 289–296.

Acta Cryst. (1980). A**36**, 450–460

X-ray and Neutron Investigations of the $P\bar{1}$–$I\bar{1}$ Transition in Pure Anorthite

BY W. ADLHART, F. FREY AND H. JAGODZINSKI

Institut für Kristallographie und Mineralogie der Universität München, Theresienstrasse 41, 8000 *München* 2, *Federal Republic of Germany*

(*Received* 10 *July* 1979; *accepted* 14 *November* 1979)

Abstract

The temperature dependence of sharp and diffuse *c* and *d* reflections in pure anorthite was investigated by X-ray and neutron measurements from room temperature up to 700 K. At 513 ± 4 K a complete, reversible and continuous phase transition $P\bar{1}$–$I\bar{1}$ can be observed. Here the diffuse scattering reaches a maximum. It has a remarkable anisotropy along the **b*** and (**a*** − **b***) directions. All experimental findings as well as the formation of an antiphase domain structure can be explained by a simple dynamical model.

0567-7394/80/030450-11$01.00

I. Introduction

Feldspars have been investigated very frequently and many publications exist on this topic (see, for example, Smith, 1974). In the case of plagioclases ($Ca_xNa_{1-x}[Al_{1+x}Si_{3-x}O_8]$), which are the subject of our investigation, the structure of the end members, anorthite ($x = 1$) and albite ($x = 0$), are rather well known. Yet with the intermediate members new structures and disorder structures occur, *e.g.* antiphase domains and exsolutions, which considerably complicate the structural interpretation (Jagodzinski &

Korekawa, 1976). Furthermore, it is commonly known that in anorthite a phase transition $P\bar{1}$ to $I\bar{1}$ occurs at about 513 K. This phase transition, as well as the phenomena of the domain structure connected with it, are the subject of our investigation.

The structure of anorthite was determined by Kempster, Megaw & Radoslovich (1962), refinements of the pure anorthite structure were carried out by Wainwright & Starkey (1971), and for room temperature and 55 K by Kalus (1978). The primitive unit cell belongs to space group $P\bar{1}$ and can be divided into four subcells, which are displaced one from another by the vectors $\frac{1}{2}[111]$, $\frac{1}{2}[110]$ and $\frac{1}{2}[001]$. These subcells differ by small deviations of the atomic coordinates (order of magnitude = 0·1 Å); in addition, pairs of subcells connected by the $\frac{1}{2}[110]$ and $\frac{1}{2}[001]$ vectors have a reversed arrangement of Al and Si tetrahedra. In view of these pseudo-symmetries, a classification of the reflections into *a* ($h + k$ = even, l = even), *b* ($h + k$ = odd, l = odd), *c* ($h + k$ = even, l = odd) and *d* ($h + k$ = odd, l = even) reflections is generally used. The average structure of the four subcells is determined by the *a* reflections and their differences by the *b*, *c*, and *d* reflections. *a*, *b*, *c* and *d* reflections are sharp in pure anorthite. Yet samples containing small amounts of albite ($x \simeq 0{\cdot}9$) reveal diffuse *c* and *d* reflections whose diffuseness depends on the concentration and the thermal and mechanical history. With rising temperature an increasing diffuseness of the *c* and *d* reflections is observed for the same samples. This rather complex behaviour caused by the albite content and the temperature has led so far to various models, where the diffuse line profiles of the *c* and *d* reflections have almost always been interpreted statically. Some authors (Heuer & Nord, 1976; Smith & Ribbe, 1969) speculate on contributions of dynamic origin (TDS).

We performed systematic investigations of anorthite with the aid of X-rays and neutrons in the temperature range 133 to 703 K. For two reasons the neutron measurements were chosen to complete the X-ray measurements. Firstly, we hoped to determine the inelastic parts of the diffuse scattering by separating the quasi-elastic and the purely elastic parts. Secondly, the influence of the Al–Si disorder can be detected more easily by neutrons than by X-rays, owing to the great difference in the scattering lengths of Al and Si. The investigated concentration range was $1 \geq x \geq 0{\cdot}95$. It must be noted that anorthites within this range are not precisely distinguished in literature. Yet our investigations indicate the great influence of even small changes of concentration. In order to distinguish clearly between the influences of the temperature and those of the albite concentration $(1 - x)$ on the diffuseness and intensity of the *c* and *d* reflections, this publication is limited to natural An_{100} (An content of 100 to 99·5%) and, in consequence, our discussion will be restricted to the temperature effect only. The results of the measurements of the concentration $1 > x \geq 0{\cdot}95$ will be discussed in a subsequent publication.

The first thorough investigation of the diffuse scattering of annealed natural and synthetic anorthites was performed by Laves & Goldsmith (1954). Electron microscopic investigations were made by several authors (Müller, Wenk, Bell & Thomas, 1973; Müller & Wenk, 1973; Müller, 1974; McLaren & Marshall, 1974). Observations of *c* domains by the dark-field-image technique were interpreted as antiphase domains with a fault vector of $\frac{1}{2}[111]$. Therefore, these domains have an influence on the line profiles of the reflections defined by $h + k + l$ = odd. The size of the *c* domains is of the order of some μm in natural anorthites, whereas smaller domains occur in the synthetic ones. Furthermore, Müller & Wenk (1973) observed that the contrast of the *c* domain boundary disappears above 473 to 523 K; on cooling to room temperature the domain structure is unchanged. Staehli & Brinkmann (1974) found with NQR measurements of pure anorthite [$An_{99.5}$, Brinkmann (1978)] a complete and reversible phase transition of a $P\bar{1}$ to an $I\bar{1}$ structure at 514 ± 4 K. This result agrees with the first neutron measurements (Frey, Jagodzinski, Prandl & Yelon, 1977), where also a complete reversible $P\bar{1}$–$I\bar{1}$ phase transition has been observed at 510 ± 1 K. Here we are only interested in this transition. Therefore, the experiments are only carried out up to about 700 K; investigations at higher temperatures are beyond the scope of this paper.

II. Experiment

All samples used in the X-ray and neutron measurements originate from the Val Pasmeda, Monzoni in South Tyrolia. These crystals have an anorthite content of about 99·5%. Because their domain size is of the order of some μm, the line profiles are not influenced. For the X-ray investigations two samples with a volume of about 1×10^{-2} mm^3 were cut from the same crystal. They had a mosaic spread of ~10′ for sample I, and ≤3′ for sample II, but twin reflections have been observed even here.

For the neutron measurements, crystals of volume about 10^3 mm^3 were used. Crystals of this size are generally twinned. The measurements of the sharp *c* reflections showed that the sample had a mosaic spread of about 50′. This figure can only be accurate to ±10′ because of the inhomogeneity of the sample.

(*a*) *X-ray investigation*

For the X-ray work, Cu$K\alpha_1$ radiation was used in connection with a cylindrically bent germanium monochromator. The Ge(111) monochromator reduces the background, avoids the $\lambda/2$ contamination and allows

for an improved resolution in reciprocal space. Weissenberg, oscillation and Noromosic (Jagodzinski & Korekawa, 1973) film techniques were used. In contrast to the oscillation photographs the crystal is held fixed in the Noromosic procedure; hence the scattered intensity can definitely be derived from a point in reciprocal space. For the oscillation and the Noromosic photographs a focusing technique was used, granting a high resolution perpendicular to the zero-layer plane (Jagodzinski, 1968). The diffractometer measurements were carried out in an ω-scan technique with an angular resolution of about 3′. In all cases, the a axis of the crystal was parallel to the goniometer axis.

The temperature of the samples was stabilized in a vacuum heater. Its technical details will be described elsewhere (Adlhart, 1980). The accuracy of the absolute temperature setting was about 5 K; however, the relative accuracy over a small temperature range and the temperature stability were about 0·3 K. Owing to the vacuum-heater, air scattering could be avoided; the long exposure times necessary for detecting weak, diffuse intensity could be achieved in this way only.

(b) Neutron-scattering investigation

All neutron-scattering investigations were carried out at the spectrometer D10 at the HFR of the ILL, Grenoble. The instrument is mounted at the end of a neutron guide so that the background is relatively small. This is essential for these experiments because of the weak, diffuse scattering intensities. The sample itself and the heating arrangement produce the main contributions to the background radiation. Scattering contributions of the furnace could be allowed for by a measurement without sample. The experiments were made at a constant wavelength of 1·44 Å [Cu(111) monochromator]. The $\lambda/2$ part within the monochromatic beam was about 5%, and disturbed the analysis of some very weak c reflections. ω scans of the c reflections in question have been made at various temperatures in a diffractometer setting ('integral' measurements) as well as in a purely elastic setting with a PG(002) analyser. In order to gain intensity the energy resolution was relatively relaxed ($\pm$0·5 THz). For each temperature point one or two a reflections were measured to get an idea of the shape of the resolution volume in reciprocal space.

For the neutron investigation a furnace with a relative temperature stability of better than $\pm$1 K during one measuring cycle was used. The accuracy on an absolute temperature scale was $\pm$4 K, the gradient within the sample crystal $\pm$1 K. Measurements were performed up to 563 K. A change of the crystal quality after finishing the experiment was not noticeable.

In order to avoid confusion we use for measurements carried out without analyser the term 'integral' in contrast to the 'elastic' one. In both cases integrated intensity means an integration in momentum space.

III. Results

(a) X-rays

First, we report on the results of the film investigations. Except for the Weissenberg photographs, where sample II was used, all the film measurements were performed with sample I.

a, b, c and d reflections have similar half-widths corresponding to the resolution of focusing oscillation photographs of about 2×10^{-3} Å^{-1} perpendicular to the zero layer line. A splitting of the reflections of the order of 10′ may be caused by twinning and mosaic effects. Fig. 1 shows a number of focusing Noromosic photographs starting from room temperature up to 703 K. The 025 c reflection of the crystal is on the Ewald sphere. Since the a axis is mounted perpendicularly to the scattering plane, the photographs show the intensity distribution of a reciprocal plane passing through the 025 reflection and lying almost parallel to the reciprocal (02$\bar{1}$) plane. Fig. 1 also shows a typical line

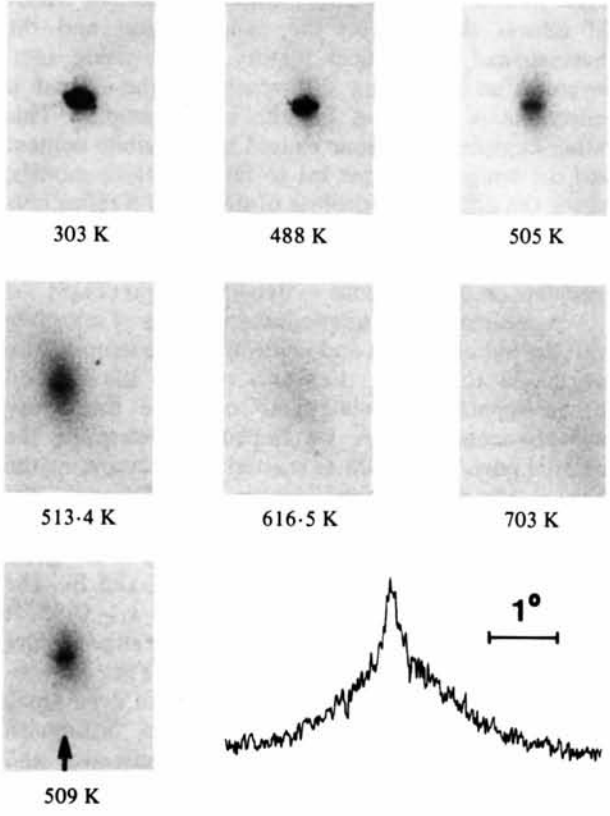

Fig. 1. Magnified area of Noromosic photographs of the 025 reflection at various temperatures. One photograph and its corresponding photometer curve are compared at 509 K. The arrow, which is parallel to the a axis, indicates the scan direction.

profile of the 025 reflection near the phase transition. These line profiles reveal sharp and diffuse contributions which can be separated visually. Fig. 2 shows the intensity of sharp and diffuse contributions as a function of temperature. On values for the sharp contribution below T $\simeq$ 490 K a large error results from overexposure of the film.

With the aid of oscillation photographs, it can be seen that just above the phase transition a scattering of rather different intensity can be observed in the position of the *c* reflections regardless of the reflection intensity below the phase transition. This behaviour is demonstrated in Fig. 3 by photometer curves of various reflections. Some reflections can be clearly separated into sharp and diffuse parts even above the critical temperature.

In Fig. 4(*a*) the diffuse scattering in the **b*c*** plane is shown by Weissenberg photographs. An oscillation photograph indicates the distribution of the diffuse scattering perpendicular to this plane in Fig. 4(*b*). The anisotropy shown in Fig. 4 holds for all *c* and *d* reflections as far as intensity could be observed. The change of the diffuse scattering as a function of temperature is also the same for all *c* and *d* reflections.

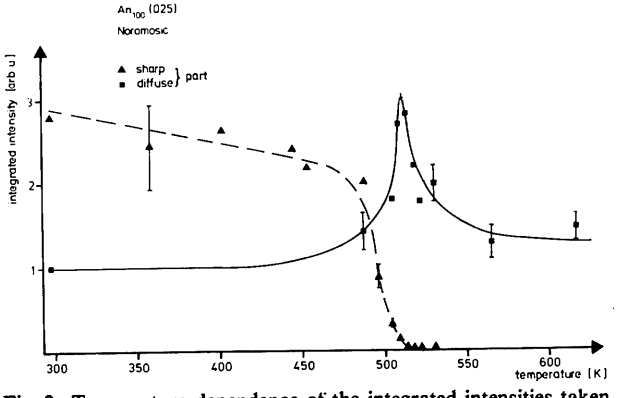

Fig. 2. Temperature dependence of the integrated intensities taken from Noromosic photographs: sharp and diffuse parts of the 025 reflection.

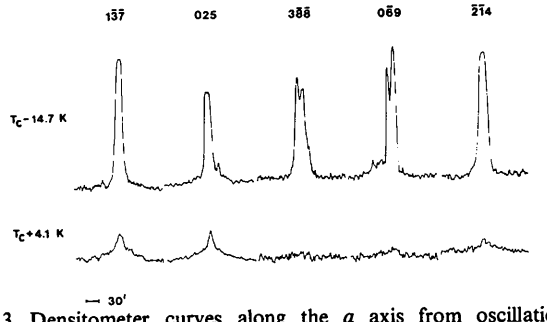

Fig. 3. Densitometer curves along the *a* axis from oscillation photographs. Comparison of various *c* and *d* reflections below and above the phase transition.

The counter measurements were carried out across the $1,\bar{7},\bar{1}3$ and $0,\bar{1}2,3$ reflections of sample I (Fig. 5). Above T_c, the intensity of the $1,\bar{7},\bar{1}3$ reflection decreases much more slowly than the intensity of the $0,\bar{1}2,3$ reflection. Fig. 6 shows a comparison of the line profiles of these two reflections. It indicates that the line profiles are qualitatively the same below T_c, but above T_c only the $1,\bar{7},\bar{1}3$ reflection line profile is slightly broadened.

The counter measurements along the 025 reflection of sample II have an angular resolution of about 3·5′. Again, the contributions to the line profile can be clearly separated below and around the phase transition (Fig. 7). In this case the line profiles were evaluated by fitting one Lorentzian and one Gaussian line with an additional constant background to the measured data (solid line in Fig. 7). The broader part corresponds to the Lorentzian profile, the sharper one to the Gaussian curve. In Fig. 8(*a*), the integrated contributions are shown as a function of temperature. Below 500 K the intensity of the diffuse part increases almost proportional to the intensity of the reflection. We assume that this fact is due to strongly tilted small mosaic blocks. These blocks are clearly visible on the Weissenberg photographs around the 042 reflection. Assuming that at room temperature the diffuse part is solely caused by the mosaic blocks, we corrected the integrated diffuse intensities by

$$I = I_D + I_C - \alpha I_S,$$

where I_S and I_D are the integrated intensities of the sharp and the diffuse contribution, I_C is the integrated contribution of the constant background below the measured curves and α is a constant defined by the ratio I_D/I_S at room temperature. The result of this procedure is a distinct maximum of I at the phase transition (Fig. 8*b*).

Fig. 9 shows the temperature dependence of the half-widths of the $1,\bar{7},\bar{1}3$, and the $0,\bar{1}2,3$ and the sharp contribution of the 025 reflections. The half-width of the $1,\bar{7},\bar{1}3$ profile increases considerably above the phase transition. The improved resolution of the 025 reflection of sample II allows for the observation of an increasing half-width of the sharp contribution too.

(*b*) *Neutrons*

Two *a* reflections (004 and 060), two *c* reflections (025 and $04\bar{5}$) and one *d* reflection (054) were measured at various temperatures. Fig. 10 shows the 060, $04\bar{5}$ and 054 reflections measured at room temperature in the purely elastic setting of the spectrometer. Gaussian-like profiles are fitted to the data. The half-widths are the same within the error range. The resolution of the instrument was determined with a better crystal. It amounted to about 15′; thus the measured profiles show essentially the mosaic effect. The measurements performed in the diffractom-

eter setting reveal obviously the same shape and the same half-width of the sample due to the dominating contribution of the sample's mosaic.

For a detailed study of the phase transition $P\bar{1}$–$I\bar{1}$ integrated intensities were calculated. They are plotted in Fig. 11 for elastic measurements. Here the temperature dependence of the *c* reflections is compared with the intensity dependence of the *a* reflection 004 which has an overall constant course up to 508 K. The slight increase of intensity of about 10% may be caused by structural variations which will be discussed elsewhere. The two *c* reflections $04\bar{5}$ and 025 have similar behaviour. The intensities decrease quickly up to 503 K. Above this temperature the decrease is much slower, but even above 513 K continuously decreasing intensity contributions remain. The error in the intensity above 613 K is quite large because of the small absolute values. These two *c* reflections show clearly a different temperature dependence above 503–513 K, compared with the $13\bar{1}$ and the $11\bar{1}$ reflections which had been measured before (Frey, Jagodzinski, Prandl & Yelon, 1977). The behaviour of the $11\bar{1}$ reflection is depicted again in Fig. 11. The temperature dependence of the 054 reflection agrees with those of *c* reflections below ~470 K. Above this temperature range the intensity was too small to be separated from the background.

The half-width of the *c* reflections $04\bar{5}$ (Fig. 12) as a function of temperature is constant up to the phase transition. Above 513 K it increases rapidly. Therefore, we tried to fit two Gaussian lines to the measured line profiles. The half-widths of the narrow one remain unchanged up to the transition temperature and agree with the value defined by the instrumental parameters and the crystal mosaic. But the width of the diffuse contribution increases considerably above T_c (Fig. 12).

Corresponding to this profile analysis the integrated intensities of the two contributions as a function of temperature are also shown separately (Fig. 13*a*). For the $04\bar{5}$ reflection the sharp contribution goes to zero roughly at 523 K; the diffuse contribution decreases also above T_c, but it can still be observed at 559 K (Fig. 14). In comparison with the $11\bar{1}$ reflection that vanishes sharply, the 'rounded' disappearance of the sharp intensity contribution is striking. The integrated

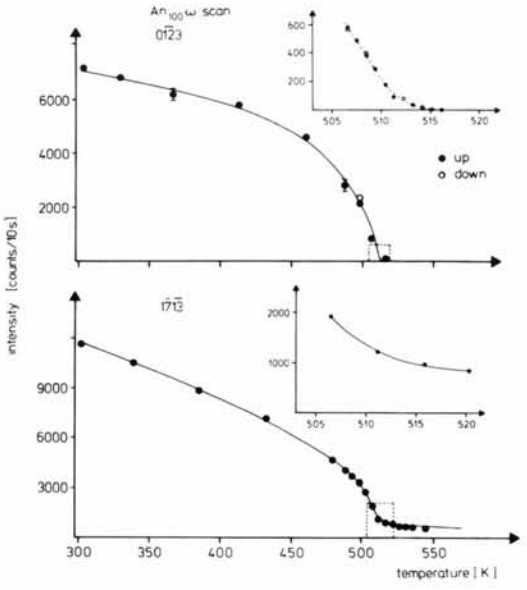

Fig. 5. Counter measurements of the intensities of the $0,\bar{1}2,3$ and $1,\bar{7},\bar{1}3$ reflections as a function of temperature.

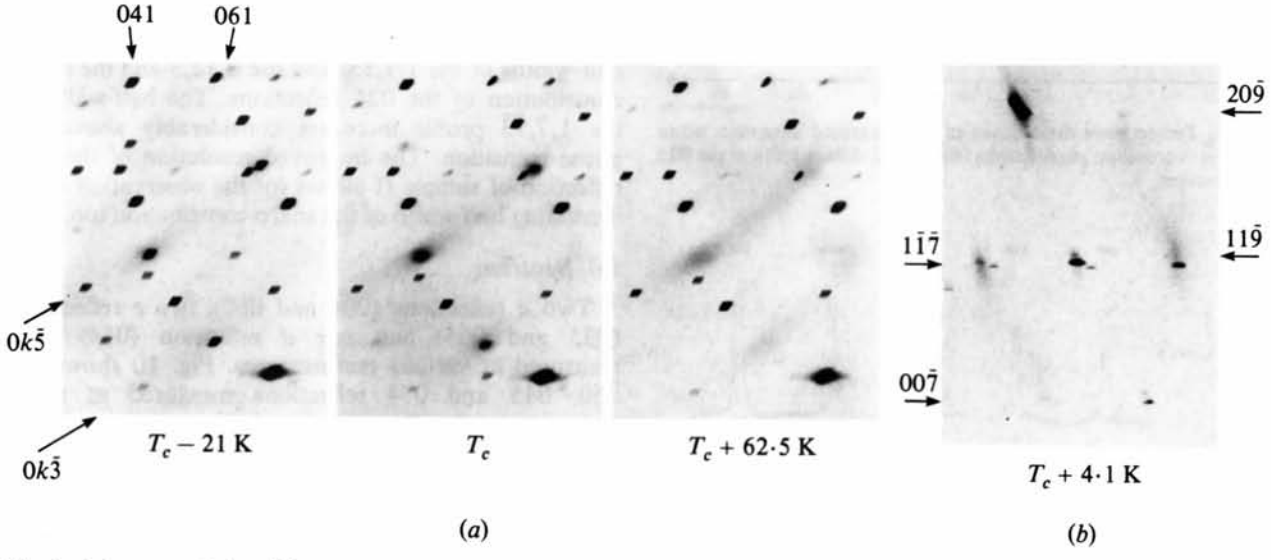

Fig. 4. Anisotropy of the diffuse scattering in An_{100} at various temperatures around T_c. (*a*) Magnified area of 0*kl* Weissenberg photographs. (*b*) Magnified area of a [100] oscillation photograph.

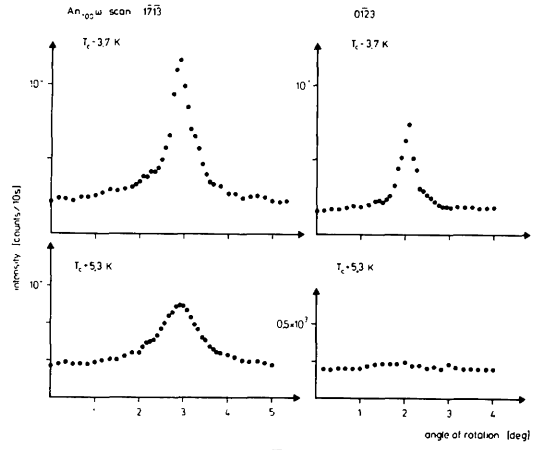

Fig. 6. Line profiles of the $1,\bar{7},\overline{13}$ and $0,\overline{12},3$ reflections recorded by counter technique (ω scan) at temperatures near the phase transition.

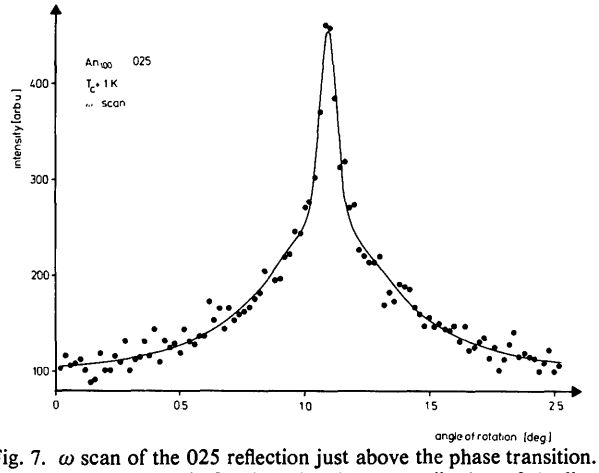

Fig. 7. ω scan of the 025 reflection just above the phase transition. A Gaussian curve is fitted to the sharp contribution of the line profile and a Lorentzian curve is fitted to the diffuse one.

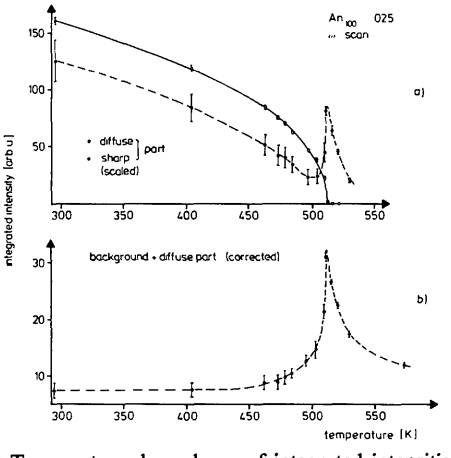

Fig. 8. (*a*) Temperature dependence of integrated intensities of the sharp and diffuse parts of the 025 reflection taken by counter measurements. (*b*) Integrated intensity of the diffuse part and the background scattering corrected for the mosaic effect.

intensity of the 025 reflection has the same temperature dependence as the 04$\bar{5}$ reflection (Fig. 13*b*). Above T_c the separation of the two intensity contributions causes problems: the intensity is increasingly dominated by a $\lambda/2$ contribution caused by the 0,4,10 reflection which cannot be separated from the sharp contribution of the 025 reflection. This problem does not exist for the 04$\bar{5}$ reflection. In this case the reflection width of the corresponding *a* reflection would indicate the $\lambda/2$ contribution, but this was not observed. Also, an estimation shows that the contribution of the weak $0,8,\overline{10}$ reflection can be neglected even above T_c. Below T_c it is no longer useful to separate the line profiles by two Gaussian lines because of the considerable uncertainty in the fitted parameters.

IV. Discussion

Our X-ray and neutron measurements indicate no different half-widths in the *a* and *c* reflections at room temperature. Therefore, an antiphase *c* domain structure that would influence *c* and *d* reflections was not observed. Corresponding to the reflection profiles, which have been measured by X-rays, possible domains would have to be larger than 3000 Å. Since the half-widths of the measured *c* reflections are not at all influenced after heating the crystal to 703 K, a change of the antiphase domain structure could not be observed either. This was expected because these changes happen only after heating the crystal to 1400–1500 K (Laves & Goldsmith, 1954; Müller & Wenk, 1973).

The temperature dependence of the *c* and *d* reflections is basically the same (Figs. 3 and 11); therefore, we do not deal with them separately in the following discussion. All investigated *c* reflections indicate a complete and reversible phase transition. The process responsible for this transition must already be started at

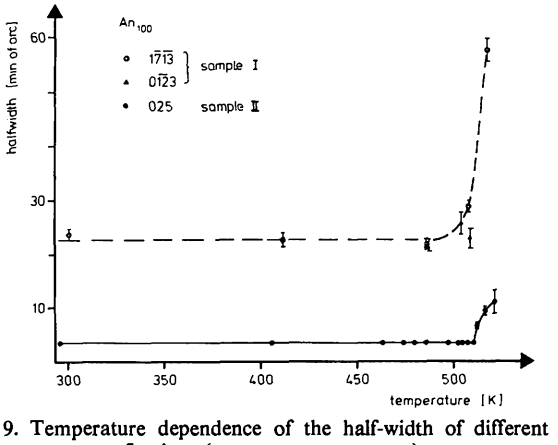

Fig. 9. Temperature dependence of the half-width of different *c* reflections (counter measurements).

room temperature because of the strong decrease of the integrated intensities there. Thus, the phase transition is already premonitored at least 200 K below the real transition temperature. As shown in Figs. 11(*a*), 13(*a*) and 13(*b*), the integrated intensities of the sharp contributions reach zero. The same holds for the X-ray measurements (see Figs. 2, 8). Therefore, an exact transition point can be determined. This fact is in contrast to models that predict *no* exact critical temperature. Since there are obviously no hysteresis effects, at least beyond $\Delta T > 1$ K, a model using energy barriers cannot be assumed either (Smith & Ribbe, 1969). In the determination of the absolute value for the transition temperature there is a small discrepancy between the X-ray and the neutron measurements, $T_c = 512 \pm 4$ and $T_c = 514 \pm 1$ K, respectively. For neutron measurements previously published (Frey, Jagodzinski, Prandl & Yelon, 1977) $T_c = 510 \pm 1$ K was found, and Staehli & Brinkman (1974) reported $T_c = 514 \pm 4$ K. Surely all these values concern the same transition point. It is of minor importance to determine the exact absolute value.

The X-ray and neutron measurements show diffuse scattering intensity for temperatures around T_c. In the X-ray photograph it can be separated visually from the Bragg contributions above and below the phase transition (Figs. 1, 3, 4). For the highly resolving counter measurements the diffuse intensity is also well separated (Fig. 7). The neutron-scattering investigations show a considerable broadening of the *c* reflection (Fig. 12) above T_c even with the purely elastic measuring procedure. However, this could only be observed in connection with the rather intense *c* reflections. A direct visual separation as for the X-ray case was not possible because of the large mosaic spread. Nevertheless, the results of fitting two Gaussian lines to the data show that the half-width of the broad line corresponds to the width of the line profile above T_c within the uncertainty corresponding to the error bars (Fig. 12). The integrated intensity of the sharp

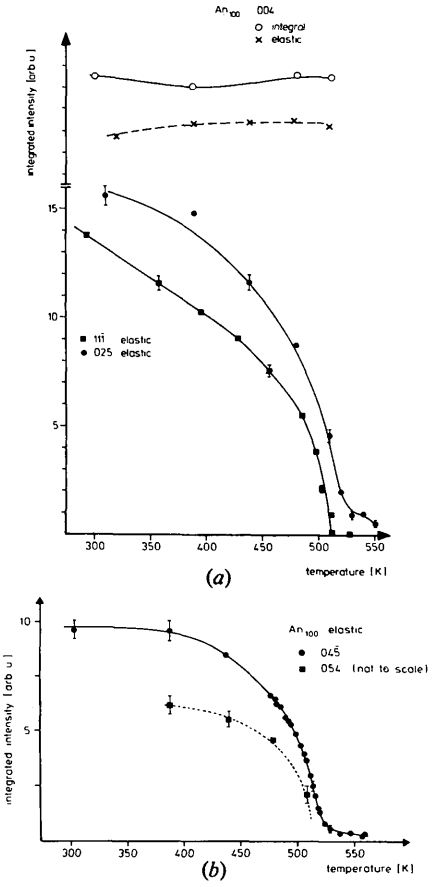

Fig. 11. Temperature dependence of integrated elastic intensities of (*a*) the 004, 025 and $11\bar{1}$ reflections and (*b*) the $04\bar{5}$ and 054 reflections.

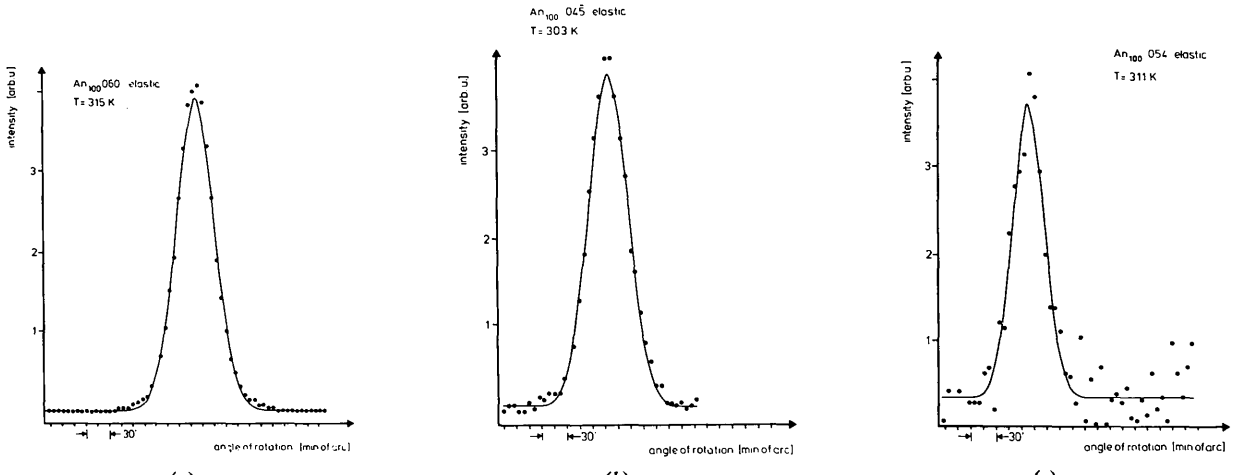

Fig. 10. Neutron measurements of (*a*) *a*, (*b*) *c* and (*c*) *d* reflections taken by the ω-scan technique with a purely elastic setting of the diffractometer roughly at room temperature.

contribution disappears at $T = T_c$ (Fig. 13). The integrated intensity of the diffuse scattering increases when approaching T_c from higher temperatures. Especially for X-rays, the increase is significant when T is close to T_c (Figs. 2, 8); less pronounced but similar behaviour was found for neutron scattering (Fig. 13). In addition, the X-ray photographs demonstrate that the distribution of the diffuse scattering is highly anisotropic: one main streak of the diffuseness corresponds to the reciprocal **b*** direction (Fig. 4*a*), another diffuse streak points along the (**a*** − **b***) direction (Fig. 4*b*). As far as we can judge from the diffraction pictures, the diffuse intensity has a similar 'wavy-band' distribution in reciprocal space to that observed in bytownites earlier. The same holds for the anorthites with a low albite content (part II). Reaching a maximum at T_c, the intensity of the diffuse scattering decreases rapidly below T_c (Figs. 2, 8). This observation was only made in X-ray work, it could not be verified by neutron scattering. If we disregard the large errors in the determination of the intensity of the diffuse background below 490–500 K, one explanation for the discrepancy could be found in the contributions of strongly tilted mosaic blocks which, as in the X-ray results (Fig. 8), prevent the decrease of the diffuse intensity at lower temperatures.

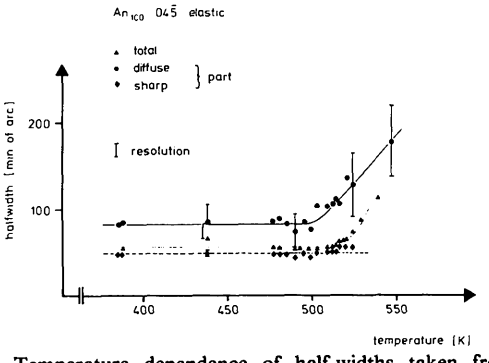

Fig. 12. Temperature dependence of half-widths taken from a profile analysis of the 04$\bar{5}$ reflection with one and two Gaussian curves.

Because of this temperature dependence of the diffuse intensity within the transition range, we assume that this intensity is of inelastic origin (thermal diffuse scattering). This does not contradict the fact that diffuse scattering can also be observed in an elastic measurement. Because of the finite energy window of the instrument, the frequency of the dynamic processes involved must be lower than 10^{12} Hz. These low frequencies contribute to an increased scattering intensity according to $I_{\text{diff}} \simeq 1/\omega^2$. Also, the X-ray measurements indicate that the distribution of the diffuse intensity within the reciprocal lattice is very broad for temperatures above 600 K. Near T_c the distribution becomes definitely sharper.

All these findings can easily be explained by a soft-mode model: a lattice mode becomes unstable, which is indicated by an anomalous decrease of the corresponding frequency, when approaching the phase-transition point. As the critical point is reached, the structure stabilizes itself by rearranging single atoms or atom groups into new positions. Thus the phase transition is continuous and reversible. Considerations of the lattice geometry dealing with the Brillouin-zone construction for the high-temperature ($I\bar{1}$) phase (Fig. 15) reveal that only a condensation of a zone-boundary phonon in the **b*** direction (Z point, Fig. 16) can be

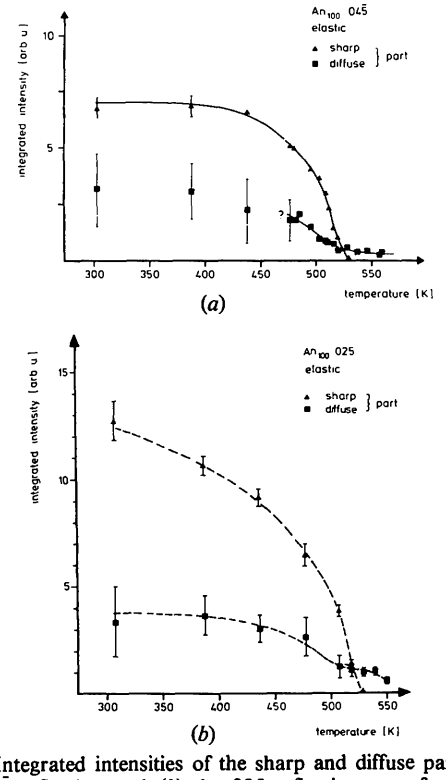

Fig. 13. Integrated intensities of the sharp and diffuse part of (*a*) the 04$\bar{5}$ reflection and (*b*) the 025 reflection as a function of temperature.

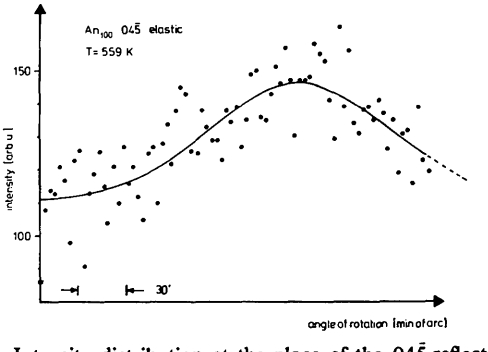

Fig. 14. Intensity distribution at the place of the 04$\bar{5}$ reflection at 559 K.

responsible because a new superstructure (c) reflection develops. This **b*** direction corresponds exactly to the direction of intense diffuse scattering (see Fig. 4a). Furthermore, Fig. 4(b) demonstrates that the (**a*** − **b***) direction also shows intense scattering along a streak between two c reflections. This result fits well the Brillouin-zone construction discussed above. An (**a*** − **b***) direction connects two Z points passing through a U point; following the discussion above the Z points are the points of unstable modes. We assume therefore that the entire dispersion branch Z–U–Z corresponds to a 'valley' in the dispersion sheet and that the higher diffuse scattering is caused by low frequencies. Γ–U'–Γ connects two a reflections and thus this direction is not equivalent to the Z–U–Z dispersion branch. Fig. 16 also shows another main difference between the connection of two Z points in the (**a*** + **b***) and (**a*** − **b***) directions. Looking at the Brillouin-zone picture coming from the low-temperature phase, we connect one c reflection to the other parallel to the (**a*** − **b***) direction. In this case the dispersion branches are affected within one Brillouin zone only, whereas a connection of two c reflections along the (**a*** + **b***) direction intersects a third Brillouin zone and crosses the connection line of two a reflections at the U' point. Several dispersion branches with an anomalously low frequency along different directions are at least not probable.

We want to emphasize that this proposed model must be proven by inelastic neutron scattering measurements. It does not seem to be easy in the case of anorthite because of its complex structure and its 312 dispersion branches. Nevertheless, a soft-mode model is a good model for a great number of compounds (Landau, 1965; Cochran, 1971; Dorner & Comès, 1977). Even for anorthite with its very complicated structure the phase transition $P\bar{1}$–$I\bar{1}$ can be explained rather easily with no further special structural assumptions. A soft phonon indicates a correlated oscillating process of at least one part of the atoms and therefore explanations assuming 'rattling' or 'bouncing' of the Ca atoms (Smith & Ribbe, 1969), leading to an uncorrelated motion, do not agree with our experimental results.

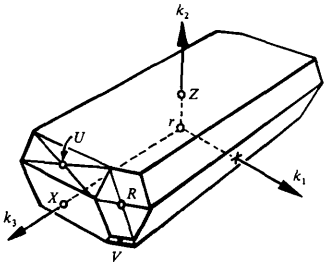

Fig. 15. Brillouin zone of a triclinic system.

One fact has not been taken into account in the discussions of our measurements so far: the X-ray measurements reveal a sharp contribution of the line profile *just above* T_c in the range $\Delta T = T - T_c \lesssim 5$ K which can be clearly separated from the diffuse background (Figs. 1, 3, 7). Correspondingly in the neutron case there exists a second Gaussian line which has the same half-width as those of the a reflections (Fig. 12) that are determined by the resolution. The integrated intensity as well as the temperature dependence of this additional scattering contribution varies for different c reflections (see Fig. 13). It leads to the observed relaxed behaviour of the intensity close to the transition point, which is typical for critical fluctuations. With respect to the continuous phase transition we assume the existence of homogeneous fluctuations with no interface energies. In a static picture we understand the short realization of small particles of the $P\bar{1}$ phase within the $I\bar{1}$ phase and *vice versa*. The size of the particles reaches a maximum at T_c and

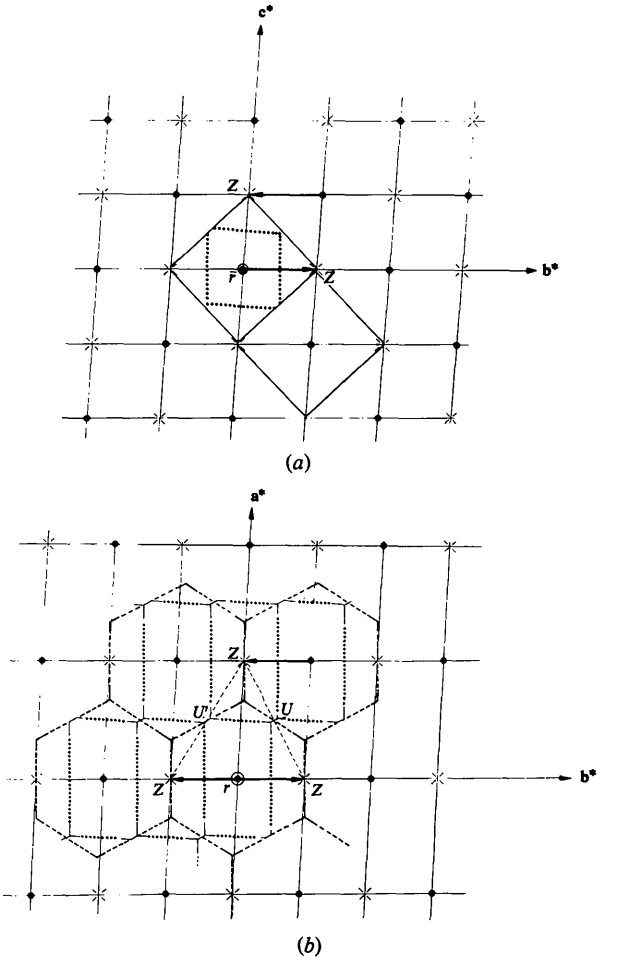

Fig. 16. (a) First Brillouin zone in the **b*c*** plane. Solid line: I phase; dotted line: P phase. (b) First Brillouin zone in the **a*b*** plane. Hatched line: I phase; dotted line: P phase.

decreases rapidly with growing temperature difference $|T - T_c|$. In this explanation the scattering intensity of the fluctuation is proportional to the difference between the structure factor of the phases ΔF. For c reflections the structure factor is zero above T_c and therefore

$$\Delta F = \sum_{\nu} f_{\nu} \exp\{2\pi i \mathbf{H}.\mathbf{r}_{\nu}(T')\},$$

where T' is a temperature just below the phase transition. The atomic positions are the sum of the equilibrium positions $\mathbf{r}_{\nu}(T)$ at $T = T_c$ and small static deviations $\Delta\mathbf{r}_{\nu}(T')$, which are defined by a condensed soft mode. If we sum over pairs of atoms that are separated by a $\frac{1}{2}[111]$ lattice translation, the structure factor reads

$$\Delta F = \sum_{\nu} f_{\nu} \exp\{2\pi i \mathbf{H}.\mathbf{r}_{\nu}\} \sin(2\pi \mathbf{H}.\Delta\mathbf{r}_{\nu})$$

$$\simeq 2\pi \mathbf{H} \sum_{\nu} f_{\nu} \exp\{2\pi i \mathbf{H}.\mathbf{r}_{\nu}\} \Delta\mathbf{r}_{\nu}.$$

Consequently, the scattering intensity is determined by the deviation $\Delta\mathbf{r}_{\nu}$ and the critical scattering should be proportional to the scattering intensity of the c reflections slightly below T_c. Yet this has not been observed (see Figs. 3, 5, 11, 13). On the contrary, the oscillating photographs allow a definite assignment of strong thermal diffuse scattering to the strong intensity of the critical scattering (see Fig. 3: 025, $1\bar{3}\bar{7}$). This scattering contribution clearly can be separated from the wide thermal diffuse scattering within reciprocal space; hence, it cannot be explained by overdamped phonons either.

The quasi-elastic origin of the scattering intensity indicates another way to explain the sharp contribution as a kind of central peak. The existence of such a response is typical for continuous displacive phase transitions which are caused by dynamical processes (Riste, 1974). To explain the 'central peak' it is generally assumed that the soft mode couples to additional phonons or impurities. Our experimental material does not allow any predictions about the kind of coupling. Yet we think that such a model best describes our results, at least in principle, for the following factors:

(*a*) No correlation between the scattering intensity below and above T_c.

(*b*) Separation of sharp and diffuse contributions above T_c.

(*c*) Correlation of intense TDS and high intensity of the sharp contribution above T_c.

More information about dynamical processes at the phase transition can be drawn from a structure determination for An_{100} at 55 and 300 K by Kalus (1978), who found a change of all atomic positions. From the continuous decrease of the intensity of the c reflections we conclude that this change is caused by continuous displacements into body-centred positions as the critical temperature is approached. Moreover, Kalus found that the thermal parameters, particularly those of two Ca atoms (Ca_{000} and $Ca_{z\bar{1}0}$), become quite anisotropic at room temperature. The main deviation lies within the **bc** plane; the amplitudes are twice as large as those of the O atoms and about three to four times larger than those of the Si–Al atoms. These observations agree well with a soft-mode model.

All atoms are involved in a soft mode but the amplitudes of the thermal vibrations may be quite different for different atoms. A definite solution of this problem by an eigenvector determination would be extremely complicated in the case of anorthite.

Of course, several dispersion branches may lower their frequencies when approaching T_c owing to the change of the force constants responsible for the soft mode. Obviously, the atomic movements corresponding to the temperature gradient of the static atomic parameters have to be correlated with these dynamic displacements. It cannot be excluded that some atomic parameters have a small discontinuity close to the critical temperature, but this was not observed within the limits of our measuring accuracy.

So far our discussion is restricted to the *P–I* transition, *i.e.* to a change in the translational group symmetry only. Any consideration concerning the centre of symmetry, which could be absent with respect to small displacement vectors either in the *P* or the *I* phase, is beyond the scope of this paper. If such a deviation occurs, it has to be discussed in connection with the fluctuations near the transition point. The average structure, however, is centrosymmetric below and above T_c.

V. Conclusions

X-ray and elastic neutron measurements up to 703 K of the *c* and *d* reflections were performed on pure anorthite. A complete and reversible continuous phase transition $P\bar{1} \rightarrow I\bar{1}$ for all structural elements occurs at a defined transition temperature. This can be concluded definitely from the vanishing sharp elastic contributions of the *c* and *d* reflections.

The diffuse scattering found by X-ray and neutron experiments has a distinct maximum at the phase transition. Because of the temperature dependence we attribute this scattering to thermal diffuse scattering. The frequency of the atomic movement must be lower than 1×10^{12} Hz within the range of the phase transition. This is indicated by the high diffuse intensity and by the fact that intensity was observed even with the elastic setting of the neutron spectrometer. An anisotropy of the diffuse scattering along the reciprocal $\mathbf{b}^*$ and $(\mathbf{a}^* - \mathbf{b}^*)$ directions was observed. This can be

explained by a 'soft-mode' model with a condensing zone-boundary phonon (Z-point mode), where the amplitudes become larger and, finally, condense out when coming from high temperatures. Different atoms can be affected in different manners. We conclude from the results of the structure refinement of Kalus that the Ca atoms mainly drive the phase transition.

Fig. 17 demonstrates schematically for one kind of atom how the phase transition can be performed. If this soft mode condenses in different parts of the crystal with a relative phase shift of π, an antiphase structure of the low-temperature phase results from it quite naturally. This behaviour is common in phase transitions of second order where the antiphase structures are energetically equivalent. Stresses occurring at the antiphase domain boundaries can be partially compensated for by impurity atoms. This aspect will be discussed thoroughly in a forthcoming paper about the phase transition of anorthites with small impurity content of albite.

It must be emphasized once again that inelastic neutron measurements are necessary to prove this phenomenological model. Therefore, our measurements can give no explanation for the microscopic reasons for the phase transition.

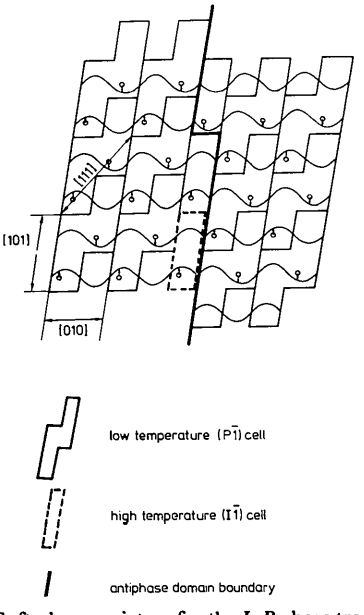

Fig. 17. Soft-phonon picture for the I–P phase transition.

The support and advice of Dr Zeyen during the neutron experiments on D10/HFR Grenoble is gratefully acknowledged. The work was supported by funds of the Bundesminister für Forschung und Technologie (Project 03-45A12I).

References

ADLHART, W. (1980). In preparation.

BRINKMANN, D. (1978). Private communication.

COCHRAN, W. (1971). *Landau's Theory on Structural Phase Transition.* In *Structural Phase Transitions and Soft Modes*, edited by E. J. SAMUELSEN, E. ANDERSEN & J. FEDER, pp. 1–13. Universitetsforlaget Oslo.

DORNER, B. & COMÈS, R. (1977). *Phonons and Structural Phase Transformation.* In *Dynamics of Solids and Liquids by Neutron Scattering*, edited by S. W. LOVESEY & T. SPRINGER, Chapter 3. Berlin: Springer.

FREY, F., JAGODZINSKI, H., PRANDL, W. & YELON, W. B. (1977). *Phys. Chem. Miner.* **1**, 227–231.

HEUER, A. H. & NORD, G. L. JR (1976). *Polymorphic Phase Transition in Minerals.* In *Electron Microscopy*, edited by H. R. WENK, Chapter 5.1. Berlin: Springer.

JAGODZINSKI, H. (1968). *Acta Cryst.* **B24**, 19–23.

JAGODZINSKI, H. & KOREKAWA, M. (1973). *Geochim. Cosmochim. Acta*, Suppl. 4, Vol. 1, 933–951.

JAGODZINSKI, H. & KOREKAWA, M. (1976). *Z. Kristallogr.* **143**, 239–277.

KALUS, C. (1978). Dissertation. Univ. München.

KEMPSTER, C. J. E., MEGAW, H. D. & RADOSLOVICH, E. W. (1962). *Acta Cryst.* **15**, 1005–1017.

LANDAU, L. D. (1965). *Collected papers of L. D. Landau*, edited by TER HAAR, pp. 193–216 (English translation). London: Pergamon.

LAVES, F. & GOLDSMITH, J. R. (1954). *Acta Cryst.* **7**, 465–472.

MCLAREN, A. C. & MARSHALL, D. B. (1974). *Contrib. Mineral. Petrol.* **44**, 237–249.

MÜLLER, W. F. (1974). *8th Int. Congr. Electron Microscopy, Canberra*, Vol. 1, pp. 472–473.

MÜLLER, W. F. & WENK, H. R. (1973). *Neues Jahrb. Mineral. Monatsh.* pp. 17–28.

MÜLLER, W. F., WENK, H. R., BELL, W. L. & THOMAS, G. (1973). *Contrib. Mineral. Petrol.* **40**, 63–74.

RISTE, T. (1974). *Anharmonic Lattices, Structural Transitions and Melting.* Leiden: Noordhoff.

SMITH, J. V. (1974). *Feldspar Minerals.* Vol. 1. *Crystal Structure and Physical Properties.* Berlin: Springer.

SMITH, J. V. & RIBBE, P. H. (1969). *Contrib. Mineral. Petrol.* **21**, 157–202.

STAEHLI, J. L. & BRINKMANN, D. (1974). *Z. Kristallogr.* **140**, 360–373, 374–392.

WAINWRIGHT, J. E. & STARKEY, J. (1971). *Z. Kristallogr.* **133**, 75–84.